Acta Geochim (2017) 36(2):339–352
DOI 10.1007/s11631-017-0151-9

ORIGINAL ARTICLE

Mineralogy, sulfur isotopes and infrared microthermometric study of the Leishan-Rongjiang antimony ore field, SW China

Jun Chen[1] · Ruidong Yang[1] · Junbo Gao[1] · Lulin Zheng[1] · Lijuan Du[2] · Minggang Yuan[3] · Huairui Wei[1]

Received: 1 January 2017 / Revised: 9 February 2017 / Accepted: 20 March 2017 / Published online: 24 March 2017

Abstract The Leishan-Rongjiang antimony ore field (LAOF) is in a unique geotectonic location in the uplift between the Youjiang and Xiangzhong basins. This paper focuses on two representative deposits in the LAOF: the Bameng and Peize antimony (Sb) deposits. We analyzed fluid inclusions (FIs) in stibnite and coexisting quartz, as well as the sulfur isotopic composition of stibnite, to better understand the nature of the ore-forming fluid and the metallogenic process. The FIs data from samples of the stibnite and coexisting quartz indicate that the ore-forming fluids were characterized by low-temperature (150–210 °C), low-salinity (1.5 wt%–6.0 wt% NaCl equiv.), and low-density (0.872–0.961 g/cm^3). The $\delta^{34}S$ values of stibnite (−8.21‰ to 3.76‰, average = −6.30‰) fall in between the sulfur isotopic compositions of the mantle and of biogenic sulfur in sedimentary rocks. However, the $\delta^{34}S_{\sum S}$ values (−4.41‰ to +0.04‰, average = −2.49‰) of the ore-forming fluids are generally closer to the sulfur isotopic composition of the mantle source, indicating that the sulfur in the LAOF was mainly sourced from the mantle, but with possible involvement of biogenic sulfur. In addition, FIs petrography and ore deposit geology show that fluid boiling resulted from an abrupt decrease in pressure, which may have triggered the precipitation of stibnite. We conclude that low-temperature, dilute hydrothermal fluids with mixed origins migrated along the regional fault and interacted with the wall rock, extracting the ore-forming materials. Then, the ore-forming fluids were injected into the fault fracture zones.

Keywords Stibnite · Fluid inclusions · Infrared microthermometry · Sulfur isotopes · Leishan-Rongjiang antimony ore field · Guizhou

✉ Ruidong Yang
rdyang@gzu.edu.cn

[1] College of Resources and Environmental Engineering, Guizhou University, Guiyang 550025, People's Republic of China

[2] State Key Laboratory of Ore Deposit Geochemistry, Institute of Geochemistry, Chinese Academy of Science, Guiyang 550002, People's Republic of China

[3] Guizhou Qinglong Antimony Mining Industry District, Qinglong Country 561400, Guizhou Province, People's Republic of China

1 Introduction

The South China antimony (Sb) metallogenic belt is the most concentrated area of antimony deposits in the world. This belt contains many mid-to-large scale antimony deposits, which can be divided from west to east into two basins: (1) Xikuangshan, Banxi, Woxi, etc. in the Xiangzhong basin; and (2) Qinglong and Banpo, Banian, etc. in the Youjiang basin (Fig. 1a). Neoproterozoic epimetamorphic rocks of southeast Guizhou Province (the exposed area of basement of the Southern China fold belt), located in the uplift between the Youjiang and Xiangzhong basins, are distributed throughout the Bameng, Dacao, Peize, and Paidiao Sb deposits (Fig. 1a). These deposits spread along a NE trend, and they are all hosted by metamorphic rocks of the pre-Sinian Xiajiang Group, referred to as the Leishan-Rongjiang Sb ore field (LAOF) (Wang et al. 1994; Fig. 1b). Over the past two decades, many studies have been carried out on the South China Sb metallogenic belt to determine the metallogenic age, the evolution of metallogenic fluid, and the sources of metallogenic material (Hu et al. 2002, 2007; Peng et al. 2002, 2003a; Su et al. 2008, 2009, 2012; Huang et al. 2011;

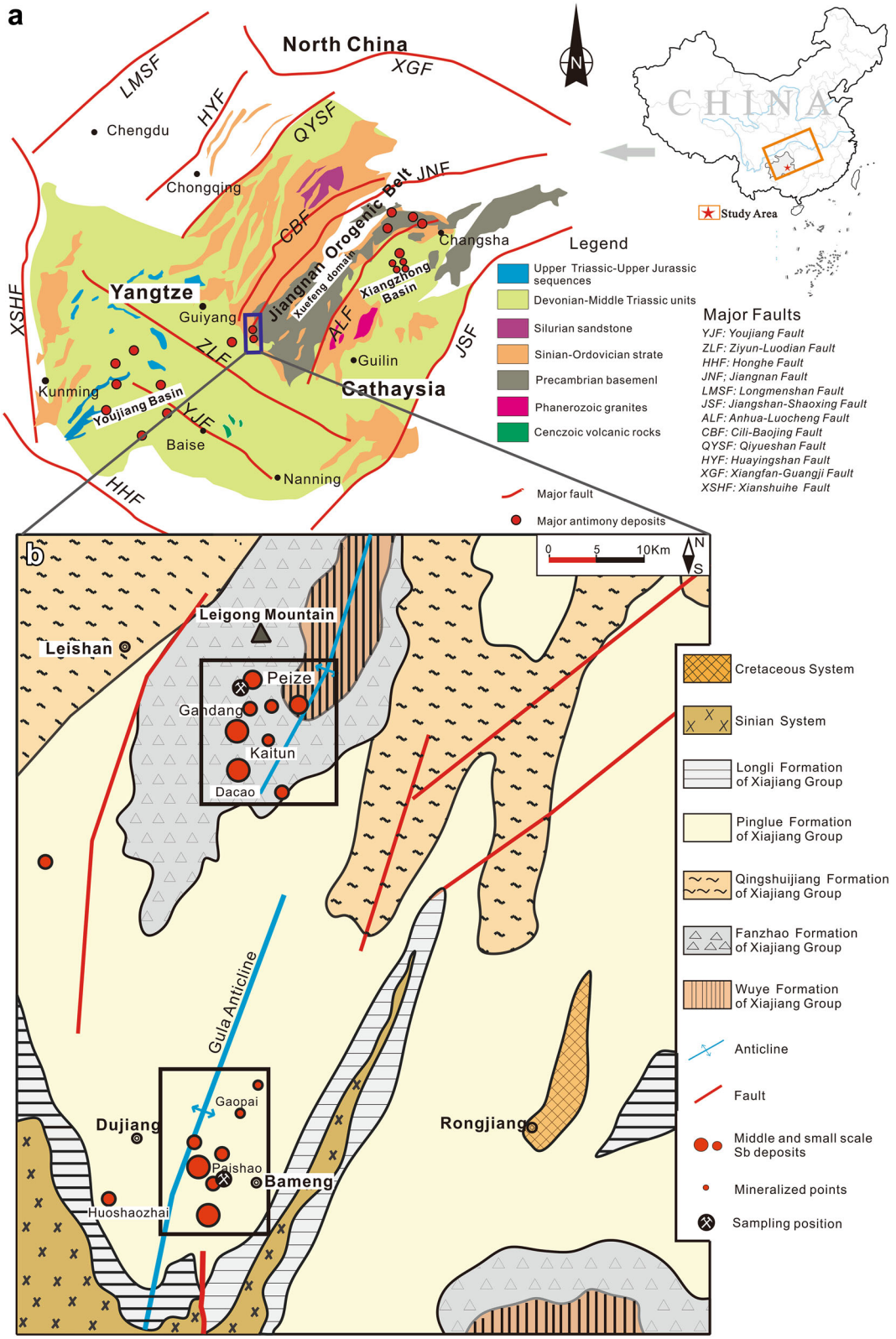

Fig. 1 Location map showing the South China antimony ore belt in SW China (**a**), and tectonic schematic map of the Leishan-Rongjiang antimony ore field (**b**) (**a** after Hu and Zhou 2012 and **b** after Wang et al. 1994)

Hu and Zhou 2012; Chen et al. 2015; Zhu and Peng 2015). However, few studies of ore deposit geology, mineralogy, and element geochemistry have been carried out on the LAOF (Zhang 1985, 1994; Chen et al. 1991; Wang et al. 1994; Zhu et al. 1999), and most held different opinions and were published in Chinese. In addition, there has been no related detailed study carried out on the nature of the ore-forming fluids or on the metallogenic mechanism of the LAOF, an omission which limits understanding of the genetic relationships between different Sb deposits in the South China Sb metallogenic belt.

Infrared microthermometry has been widely applied in geology in recent years, especially in the study of metallic minerals (e.g., stibnite, pyrite, enargite, wolframite) (e.g., Campbell and Panter 1990; Mancano and Campbell 1995; Kouzmanov et al. 2002). These minerals can be directly observed and analyzed to determine the geophysical and geochemical conditions of the ore-forming fluid (Buchholz et al. 2007; Ge et al. 2011; Ni et al. 2014, 2015; Sun et al. 2014, 2015; Zhu and Peng 2015). Here we present a systematic mineralogic study of the fluid inclusions (FIs) in stibnite and coexisting quartz and the sulfur isotopic geochemistry of stibnite of the Peize and Bameng Sb deposits. As these two deposits are representative deposits in the LAOF, our analysis provides a springboard to discuss the nature of the ore-forming fluids and the metallogenic process in the region.

2 Regional and ore-deposit geology

2.1 Geologic setting

Since the Wuling orogeny, crustal rigidity in southeastern Guizhou Province has increased. At the end of the late Proterozoic, the study area completed the process of cratonization (Wang et al. 1994). Multi-period tectonic movement in this area formed NNE-oriented large-scale circular and linear structures. The circular structures correspond to the large complex folds (Leigongshan anticline) controlling these deposits (Fig. 1b); the linear structures correspond to deep faults (i.e., the Songtao-Rongjiang deep fault) and to dykes. For example, a large number of lamprophyre and alkaline ultrabasic dykes are exposed in the Leigongshan area along the east side of the Songpan-Rongjiang faults, which are a part of the Hubei-Hunan-Guizhou lithospheric faults. However, the relationship between these rock bodies and the antimony veins is still not clear.

2.2 Geology of the Bameng and Peize deposits

The LAOF contains several Sb deposits, namely, the Peize, Gandang, Kaitun, and Dacao in the north; and the Bameng, Huoshaozhai, Paishao, and Gaopai in the south (Fig. 1b). The Bameng Sb deposit is the largest and accounts for 70% of the LAOF Sb reserves (Zhu et al. 1999). The exposed strata in the ore field mainly include the pre-Sinian Xiajiang Group, which has an angular unconformable contact with the underlying Sibao Group. From bottom to top, the Xiajiang Group can be divided into the Jialu, Wuye, Fanzhao, Qingshuijiang, Pinglüe, and Longli Formations. The Pinglüe and Fanzhao Formations are the ore-hosting strata of the Bameng and Peize Sb deposits, respectively. Igneous rocks are scattered within the ore field as small plutons and dykes. According to isotopic age data (No. 104 geological team of the Bureau of Geology and Mineral Resources of Guizhou Province), the emplacement age of these igneous rocks has a wide range and is different from the mineralization age of antimony. The deposits in the LAOF are mainly controlled by the Gula anticline (Fig. 1b), but the ore bodies are significantly controlled by faults (Fig. 2) and mostly occur as lenticular and vein-like shapes 60–650 m in length and 10–30 m in width, with dip angles of 40°–45° (Chen et al. 1991). The ore bodies that have widespread silicification always occur as veins in the fracture zone of steep faults and in the interlayer fracture zone (Fig. 2).

The mineral assemblages of different antimony deposits in the LAOF are generally similar. Ore minerals are dominated by stibnite (Fig. 4a–h) and pyrite (Fig. 4a, d) with minor sphalerite, chalcopyrite, and arsenopyrite (Wang et al. 1994); the gangue minerals include quartz (Fig. 4a–f), calcite (Fig. 4e), and minor amounts of ankerite (Fig. 4b), sericite (Fig. 4a), and pyrophyllite (Fig. 4h). Detailed mineralogical features have been documented (Zhang 1985, 1994; Wang et al. 1994; Zhu et al. 1999). The deposits of the LAOF can be divided into three types: stibnite-quartz, stibnite-quartz-calcite, and stibnite-quartz-pyrite, showing that the quartz is closely related to Sb mineralization. Common ore textures include brecciated (Fig. 3a), massive (Fig. 3b), fine-grained (Fig. 3c), disseminated (Fig. 3d), and especially replacement structures, showing characteristic hydrothermal alteration. At the LAOF, Sb mineralization is spatially associated with silicification and dolomitization. In addition, pyritization, sericitization, and silicification occur in wall rocks from the alteration center to the edge (Fig. 4a).

Events recognized at the Bameng and Peize deposits include pre-ore, main-ore, and late-ore stages, of which the former two are associated with the Sb mineralization. The pre-ore stage is characterized by finely-disseminated stibnite in the silicified wall rocks (Stb-I) (Figs. 3d, 4g, h). At the main-ore stage, the minerals included quartz and stibnite (Stb-II) with euhedral to subhedral crystals and grain sizes between 0.8 and 10 mm (Fig. 3a–c). Ankerite, pyrophyllite, and sericite were the hydrothermal alteration

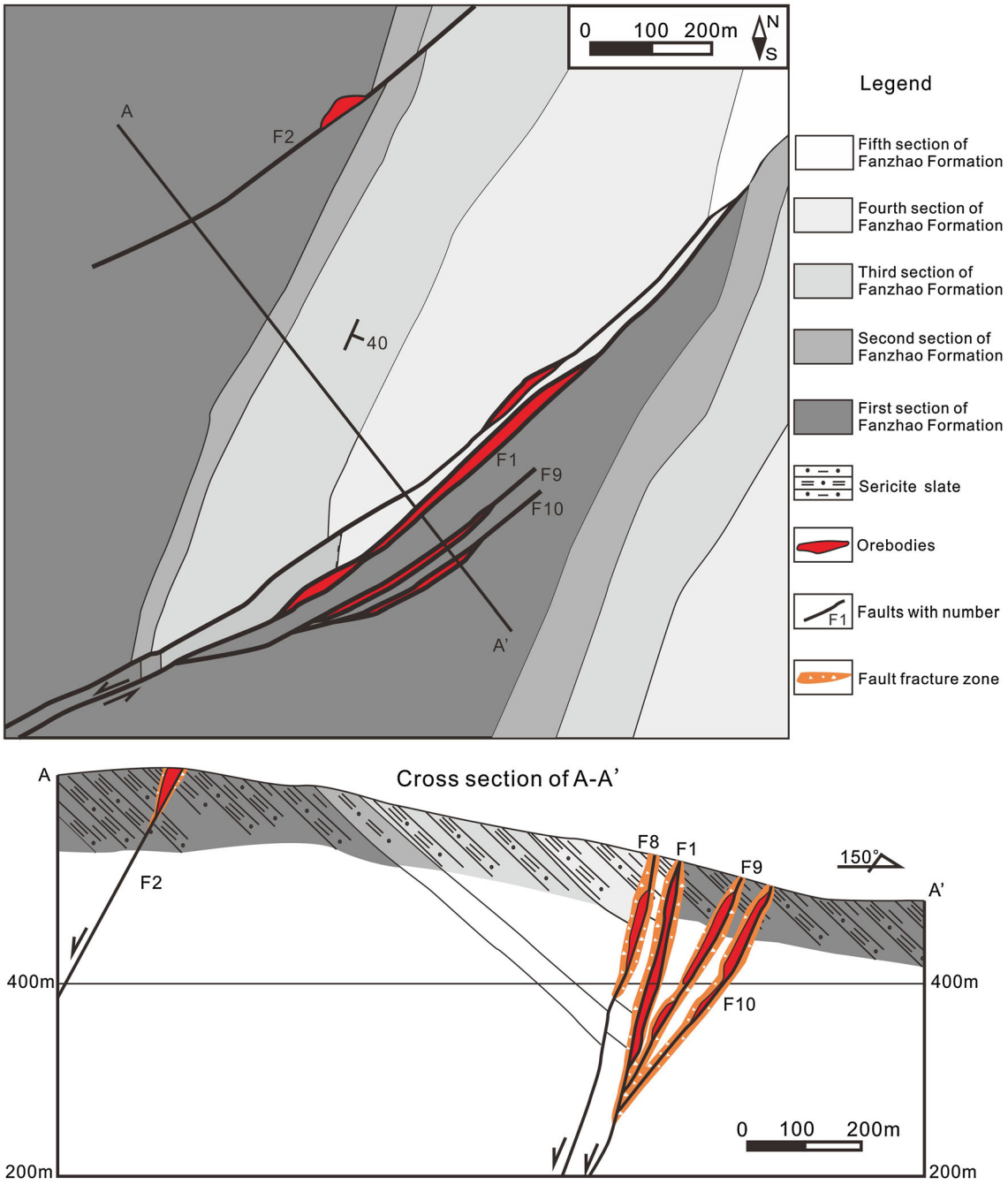

Fig. 2 Geological map of the Bameng Sb deposit in the Leishan-Rongjiang antimony ore field (modified from Wang et al. 1994)

products in this stage (Figs. 3a–c, 4a–b, h). At the late-stage, minor pyrite appeared in the fine veins (Fig. 4d).

3 Analytical methods

Samples were collected from the Bameng and Peize Sb deposits, and examined and analyzed using an electron probe micro analyzer (EPMA) to identify the chemical compositions and paragenesis of the minerals. All of the FI studies were carried out in the State Key Laboratory of Ore Deposit Geochemistry, Institute of Geochemistry, Chinese Academy of Sciences. Microthermometric measurements were obtained using a Linkam THMSG600 heating-freezing stage attached to an Olympus BX51 infrared microscope connected to a ROLERA-XR infrared digital camera. The estimated temperature measurement accuracy was ±0.1 °C. The rate was ≤15 °C/min, and from 0.1 to 1 °C/min near the phase transition point. To minimize the effects of infrared light heat on the homogenization and freezing

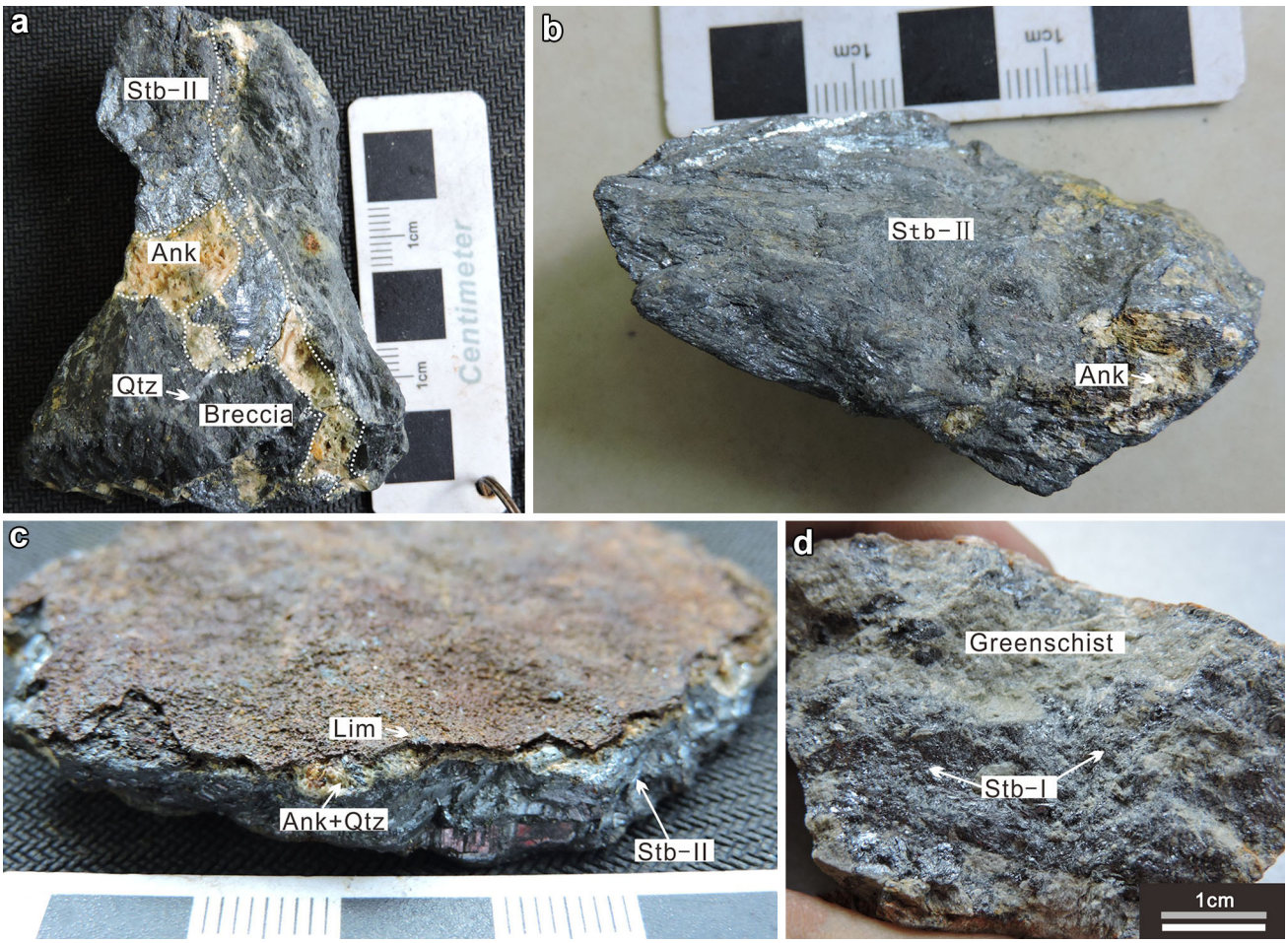

Fig. 3 The main structures and tectonics of antimony ores of the Leishan-Rongjiang antimony ore field. **a** Breccia ore. **b** Drusy ore at the main-ore stage (Stb-II). **c** Bedded orebody in fault zone and altered minerals including ankerite, kaolinite, and limonite. **d** Disseminated ore of greenschist rocks at late-ore stage (Stb-I)

point temperatures of FIs, we set the infrared light intensity as low as possible during the course of the experiment (Ge et al. 2011). Additionally, in the freezing experiment of the medium and low-salinity inclusions, we first carried out uniform heating, followed by freezing, to prevent the leakage of inclusion due to freezing expansion (Su et al. 2015).

Stibnite was crushed to 200 mesh using an agate mortar for sulfur isotope analysis, which was performed at the State Key Laboratory of Ore Deposit Geochemistry, Institute of Geochemistry, Chinese Academy of Sciences. The samples were reacted with heated CuO to produce sulfur dioxide, and their $\delta^{34}S$ values were measured by a Thermo Finnigan MAT-253 mass spectrometer. The results are expressed as $\delta^{34}S$ relative to the Vienna Canyon Diablo Troilite (V-CDT). The analytical precision was ±0.1‰.

Mineral compositions were determined using an EPMA-1600 operated with an accelerating voltage of 25 kV, a beam current of 10 nA, and an ablating diameter of 10 μm at the State Key Laboratory of Ore Deposit Geochemistry, Institute of Geochemistry, Chinese Academy of Sciences.

4 Results

4.1 Mineral chemistry

We carried out the EPMA analysis for stibnite and pyrite at the main-ore and late-ore stages, respectively. The test results are in Table 1. Sulfur content in the stibnite samples averaged 26.93% and Sb content averaged 71.38%. Arsenic was the main accompanying element, with an average content of 2.47%, which is similar to that of the stibnite (2.12%–2.99%) in the Woxi Au–Sb–W deposit in the Xuefengshan Range (Zhu and Peng 2015). In addition, As can displace S, causing the loss of S in the stibnite. Moreover, some of the data indicate that the sulfophilic elements, such as Cu and Zn, are associated with stibnite, indicating

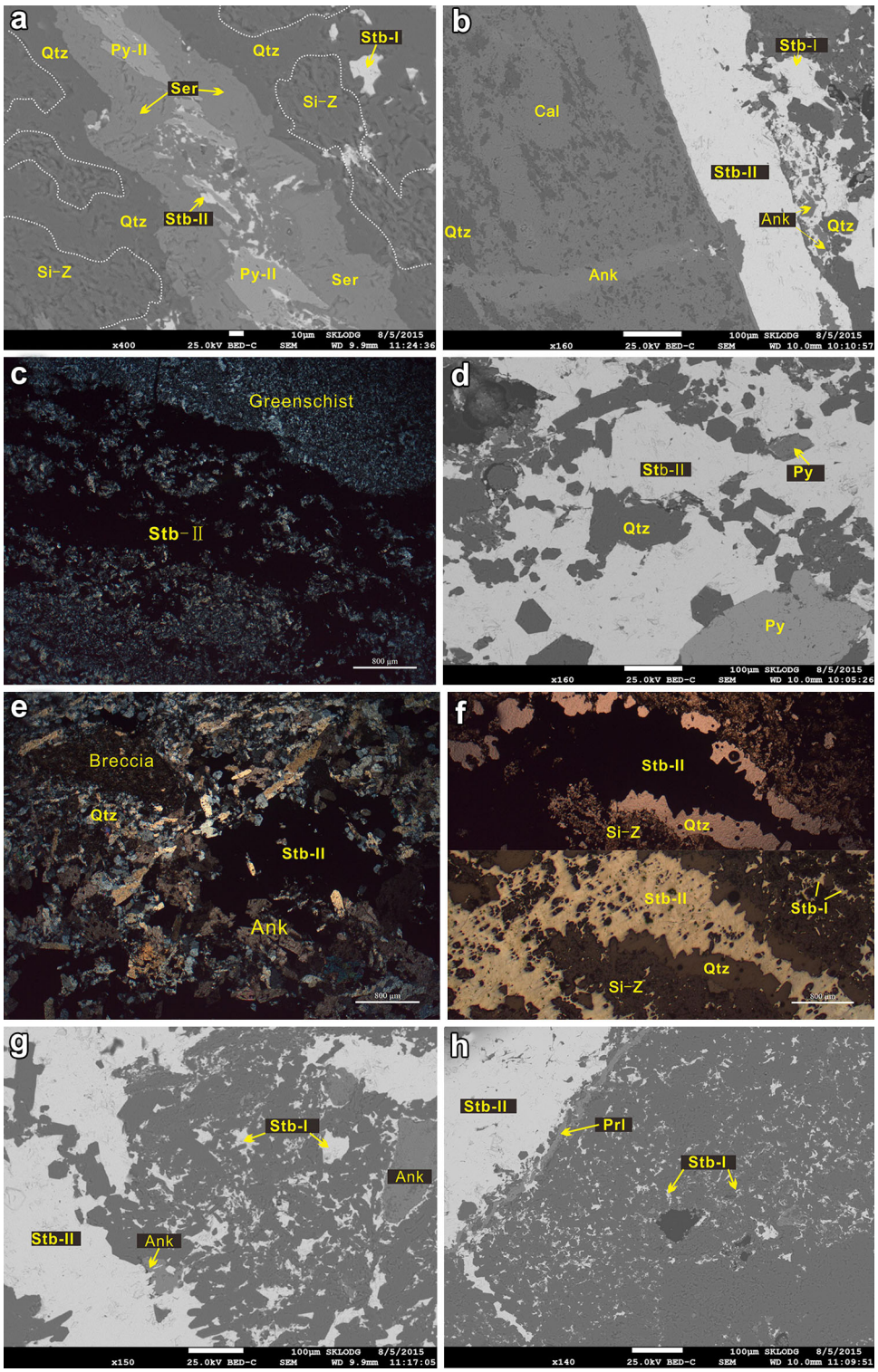

Fig. 4 Photomicrographs of metallic and gangue minerals from the Leishan-Rongjiang antimony ore field. **a** Alteration zone changes from sulfide, sericite, quartz, and silicification belts from center to edge. **b** Stibnite-II vein cuts across the quartz-ankerite-stibnite ore. **c** Vein-like stibnite cuts across greenschist. **d** Subhedral pyrite filled in the quartz-stibnite ore. **e** Stibnite-II formed in breccia ore. **f** Stibnite-II and coexisting quartz. **g**, **h** Fine-grained and anhedral stibnite-I and coarse-grained and subhedral stibnite-II. *Stb* stibnite, *Qtz* quartz, *Py* pyrite, *Ser* sericite, *Si-Z* silicification zone, *Ank* ankerite, *Cal* calcite, *Prl* pyrophyllite

that these elements were probably enriched in the ore-forming fluid during the main stage of Sb mineralization.

The late-ore stage samples were characterized by minor pyrite. Iron content in the pyrite averaged 45.69%; S content averaged 53.78% (Table 1). In addition, pyrite generally contained trace Sb (averaging 0.14%) as well as As (averaging 0.58%), albeit in a concentration much lower than that in stibnite. Gold content of the pyrite averaged 0.03%, suggesting that Au mineralization probably occurred in the same stage as pyrite precipitation and that the precipitation of Au may have been caused by the decrease in As content in the ore-forming fluid. The Au-

Table 1 Representative electron probe micro analyzer data of stibnite and pyrite in the Leishan-Rongiang antimony ore field (wt%)

Mineral	Stage	Point	S	Fe	Sb	As	Au	Cu	Zn	Ag	Pb	Total
Stibnite	Main-ore	sb1	27.19	bdl	71.93	2.11	0.02	0.02	bdl	bdl	bdl	101.27
		sb2	26.98	bdl	71.99	2.83	bdl	bdl	0.03	bdl	bdl	101.84
		sb3	26.92	bdl	71.58	2.54	bdl	0.03	bdl	bdl	bdl	101.07
		sb4	26.86	0.02	71.48	2.77	bdl	0.06	0.04	0.02	bdl	101.24
		sb5	26.81	bdl	71.23	2.06	bdl	0.04	bdl	bdl	bdl	100.14
		sb6	26.66	bdl	71.06	2.47	bdl	bdl	0.02	bdl	bdl	100.21
		sb7	27.20	bdl	70.39	2.83	bdl	0.03	bdl	bdl	bdl	100.46
		sb8	26.83	bdl	70.90	2.12	bdl	0.02	0.02	bdl	bdl	99.89

Mineral	Stage	Point	S	Fe	As	Au	Se	Ni	Co	Sb	Te	Zn	Total
Pyrite	Late-ore	py1	53.36	45.35	0.69	bdl	bdl	bdl	bdl	0.29	bdl	bdl	99.69
		py2	53.16	45.52	0.56	0.09	0.03	0.02	bdl	bdl	bdl	bdl	99.38
		py3	53.89	46.34	0.52	bdl	bdl	0.02	bdl	0.02	bdl	bdl	100.80
		py4	53.35	45.57	0.59	bdl	bdl	bdl	bdl	0.59	bdl	bdl	100.10
		py5	54.42	46.09	0.61	bdl	bdl	bdl	bdl	bdl	bdl	bdl	101.13
		py6	54.19	46.31	0.63	0.02	bdl	bdl	bdl	0.10	bdl	bdl	101.26
		py7	54.09	45.19	0.57	0.03	0.03	0.02	bdl	0.07	bdl	bdl	99.99
		Py8	53.24	44.98	0.56	0.04	bdl	0.03	bdl	0.04	bdl	bdl	98.90
		Py9	54.36	45.85	0.50	0.02	bdl	bdl	bdl	0.05	bdl	bdl	100.78

bdl below the detection limit (200 ppm)

bearing pyrite has little economic value due to low contents in the deposit.

4.2 Fluid inclusion petrography

The stibnite-quartz type ore was chosen for analysis of the main-ore stage. Quartz displayed a close paragenetic relationship with stibnite (Fig. 4e–f). Using the standard for identifying primary, secondary, and pseudosecondary inclusions by Roedder (1984) and Lu (2014), this paper mainly focuses on primary FIs in the LAOF.

Type-I FIs consisted of a vapor bubble and a liquid phase (Fig. 5a–c). These FIs were negative crystals, usually having long columnar and irregular short columnar shapes. The vapor phase occupied between 5 and 30% of the inclusion volume and homogenized into a liquid phase. The sizes of the inclusions ranged from 12 to 30 μm (long axis). Type-I FIs were abundant in stibnite samples and distributed along the {010} cleavage plane of the stibnite crystal.

Type-II FIs (two-phase) were observed randomly as irregular shapes that developed in both stibnite and quartz. These FIs in stibnite and quartz were subdivided into Type-IIa and Type-IIb, respectively.

Type-IIa FIs appeared as isolated inclusions in stibnite as oval and irregular polygons with sizes of 10–40 μm. Vapor accounted for approximately 25% of the total volume of the inclusions (Fig. 5d, e).

Type-IIb FIs were scattered, mostly as oval and irregular shapes, with sizes of 6–13 μm. Vapor accounted for approximately 10–40% of the total volume of the inclusions and homogenized into a liquid phase (Fig. 5g–i).

Type-III included aqueous daughter minerals, sparsely distributed with Type-IIb in quartz, with sizes of 10–12 μm (Fig. 5h).

Clusters of primary FIs forming at the same time show considerably variable liquid/vapor ratios and generally exhibit roughly similar homogenization temperatures, suggesting that they form during the boiling of fluid (Roedder 1984; Lu et al. 2004). Similarly, this type of FIs occurred in stibnite samples (Fig. 5d, f), indicating that fluid boiling may have been a key factor responsible for the precipitation of stibnite during the main-ore stage.

4.3 Results of microthermometry

The phase transformation process of FIs in stibnite and quartz during temperature measurement is shown in Fig. 6.

The Type-I FIs had melt temperature of ice (Tm-ice) values ranging from −0.9 to −3.2 °C and salinity varying from 1.57 wt% to 5.26 wt% NaCl equiv. (n = 43, mean = 3.61 wt% NaCl equiv.), with a peak value of 3.0 wt%–4.5 wt% NaCl equiv (Fig. 7b). Homogenization temperature values ranged from 142 to 210 °C (n = 49, mean = 171 °C) with a peak value between 160 and 180 °C (Fig. 7a). Bulk densities (Table 2) averaged 0.921 g/cm^3.

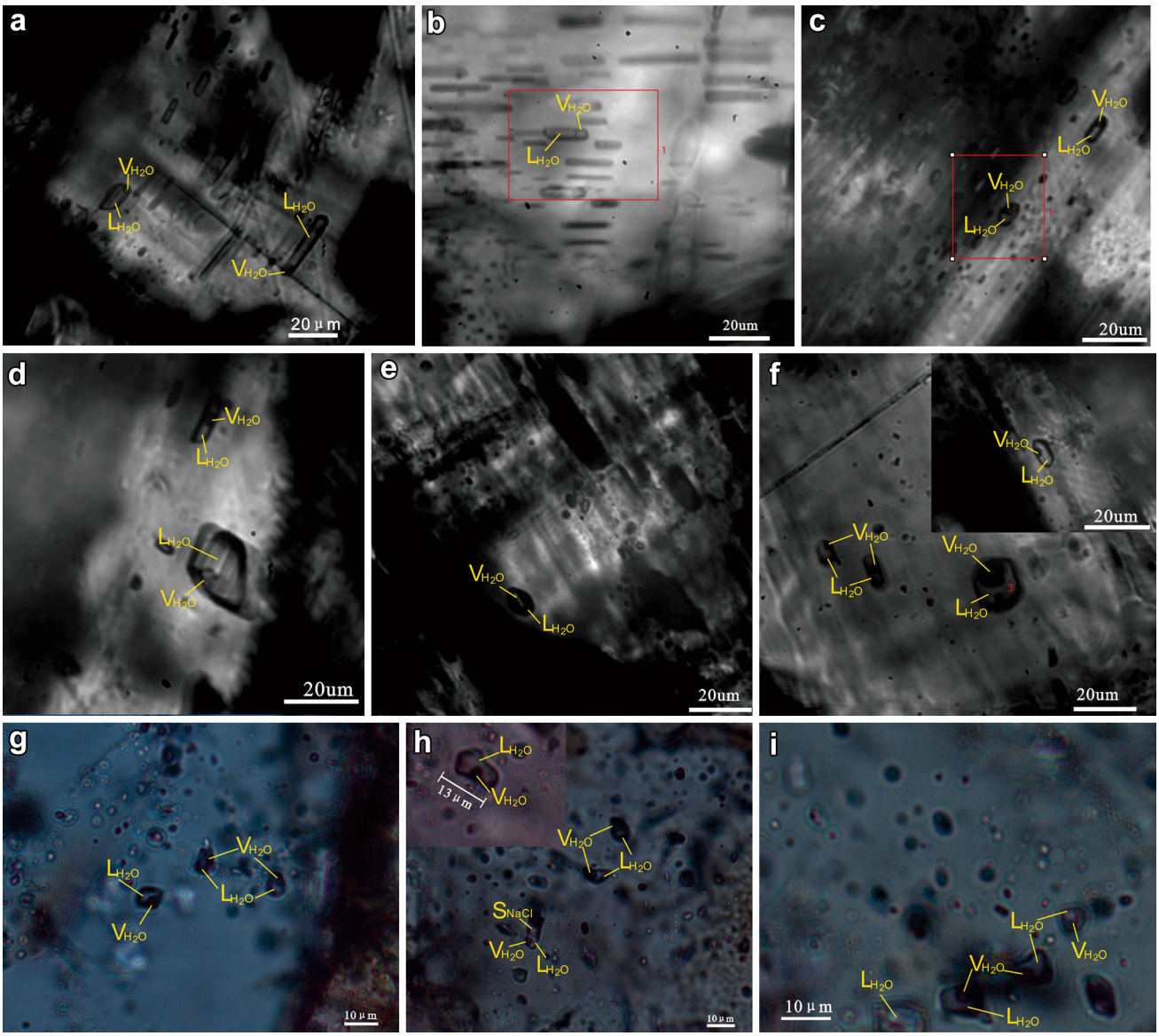

Fig. 5 Photomicrographs of representative fluid inclusion types at room temperature in stibnite and coexisting quartz. **a–c** Type-I mass fluid inclusions in stibnite; **d–f** Type-IIa individual fluid inclusions in stibnite; **g–i** Type-IIb fluid inclusions in quartz

The Type-IIa FIs had Tm-ice in the range of −1.2 to −2.3 °C, corresponding to salinities of 2.07–4.65 wt% NaCl equiv. (n = 13, mean = 3.55 wt% NaCl equiv.), with peak values varying from 3.0 to 4.0 wt% NaCl equiv (Fig. 7b). Their homogenization temperature values mostly ranged from 155 to 184 °C (n = 13, mean = 161.97 °C) with a peak value between 150 and 180 °C (Fig. 7a). Bulk densities (Table 2) averaged 0.934 g/cm^3.

For the type-IIb FIs, Tm-ice ranged from −1.1 to −3.6 °C, and salinities mostly varied from 1.91 to 5.86 wt% NaCl equiv. (n = 26, mean = 3.81 wt% NaCl equiv.) with two peak values (Fig. 7d). The main peaks ranged from 3.1 to 4.5 wt% NaCl equiv. whereas the sub-peak values were from 2.0 to 2.5 wt% NaCl equiv., consistent with the peak value of the Type-IIa inclusions (Fig. 7b). Type-IIb homogenization temperature values ranged from 138 to 252 °C (n = 26, mean = 172.8 °C), with two peak values ranging from 150 to 160 °C and from 170 to 190 °C (Fig. 7c). Bulk densities (Table 2) averaged 0.922 g/cm^3.

4.4 Sulfur isotopes

Eight stibnite samples were collected for sulfur isotope analysis (Table 3). Their $\delta^{34}S$ values averaged −6.30‰, with a range of 4.45‰. The $\delta^{34}S$ values of coexisting fluids ($\delta^{34}S_{\sum S}$) are related to temperature, pH, and fO_2 during sulfide precipitation (Ohmoto and Rye 1979). The LAOF

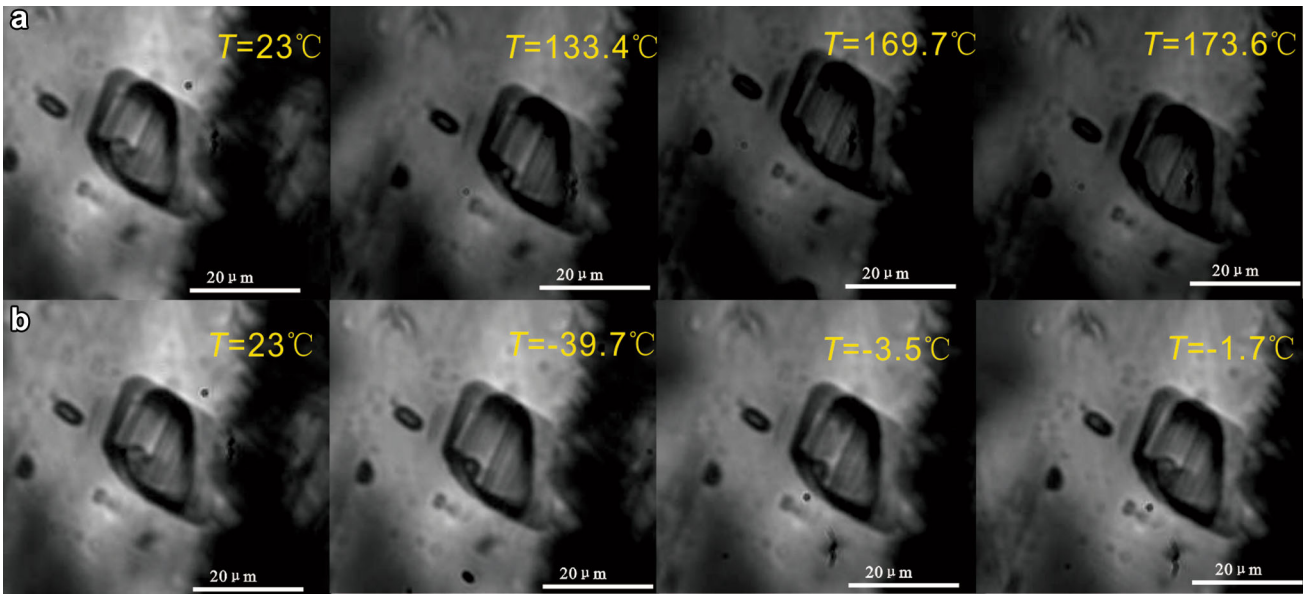

Fig. 6 The homogenization temperature (**a**), and the final ice-melting temperature (**b**) behavior of fluid inclusions in stibnite

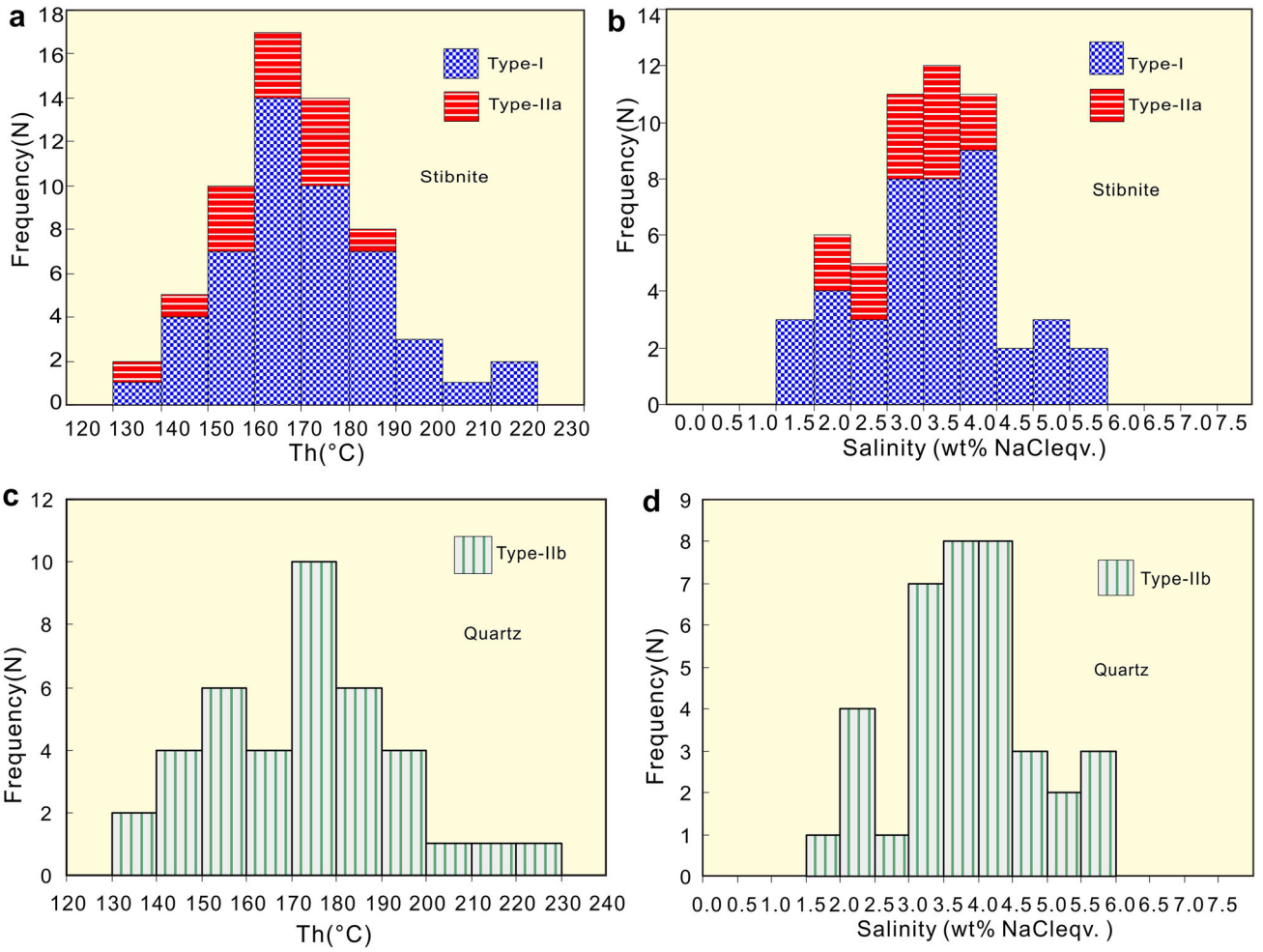

Fig. 7 Histograms of salinities and homogenization temperatures of fluid inclusions in stibnite (**a**, **b**), and coexisting quartz (**c**, **d**), collected from the Leishan-Rongjiang antimony ore field

Table 2 Microthermometric data for the Leishan-Rongiang antimony ore field

Mineral	Type	No.	Fill (%)	Tm-ice (°C)	Th (°C)	Salinity (wt% NaCl eqv.)	D (g/cm^3)
Stibnite	I	6	8–15	−0.9 to −1.8	142–170	1.57–3.06	0.917–0.943
	IIa	9	5–10	−1.9 to −2.3	155–174	3.23–4.65	0.920–0.947
	I	12	6–12	−2.2 to −2.5	140–188	3.71–4.18	0.972–0.959
	I	23	5–10	−2.1 to −2.6	153–170	3.55–4.34	0.872–0.915
	I	8	6–12	−2.3 to −3.2	167–210	3.87–5.26	0.912–0.936
	IIa	4	5–15	−1.2 to −1.8	173–184	2.07–3.06	0.907–0.936
Quartz	IIb	26	20–40	−1.3 to −3.6	138–196	2.24–5.86	0.876–0.958
	IIb	13	20–40	−1.1 to −3.5	155–252	1.91–5.71	0.943–0.961

We obtained the salinities of type-I and type-II inclusions according to the tables of melt temperatures of ice by Bodnar (1993) and Lu et al. (2004). Other relevant parameters are based on the parameter calculation software for inclusions by Brown and Lamb (1989)

No number of measurements, *Tm-ice* melt temperature of the ice, *Th* homogenization temperature, *D* density

Table 3 Sulfur isotopic compositions of stibnite collected from the Leishan-Rongjiang antimony ore field

Stage	Sample	$\delta^{34}S_{CDT}$/‰	$\delta^{34}S$ H_2S/‰
Pre-ore	LS-1	−8.21	−4.41
	LS-7	−7.21	−3.41
	LS-8	−5.84	−2.04
	PZ-1	−6.37	−2.57
Min-ore	LS-2	−6.5	−2.45
	LS-3	−6.26	−2.46
	PZ-4	−6.48	−2.68
	PZ-5	−3.76	0.04
Average		−6.30	−2.49

Analyst: Gu Jing

samples had an assemblage of stibnite and pyrite, but lacked sulfates, indicating relatively low fO_2 conditions (Ohmoto 1972) and fluids dominated by H_2S. Previous studies have shown that temperature has a subtle effect on the $\delta^{34}S$ value of H_2S when H_2S is the dominant species of S in the ore-forming fluid. Therefore, the $\delta^{34}S$ values of H_2S likely closely reflect the bulk fluid values (Ohmoto and Rye 1979; Saravanan and Mishra 2009). We calculated $\delta^{34}S$ H_2S values of H_2S based on the fractionation factors [$1000\ \ln\alpha(Sb_2S_3–H_2S) = -0.75 \times 10^6/T^2$] of Ohmoto and Goldhaber (1997) and the average temperature of the stibnite fluid inclusions (171 °C) (Table 3).

5 Discussion

5.1 Sources of sulfur

Calculated $\delta^{34}S_{\sum S}$ values of the LAOF ore-forming fluid (Table 3) are close to the $\delta^{34}S_{\sum S}$ values of the Woxi (−5.85‰ to −0.90‰) and Wangjiacun (−4.16‰ to −2.1‰) antimony deposits in the Xiangzhong basin (Bao 1989; Bao et al. 1999; Gu et al. 2004; Xiao 2014), indicating that these deposits probably have similar sulfur sources. Previous studies suggest that hydrothermal sulfur has three potential sources (Ohmoto 1972; Zheng 1991; Seal 2006): (1) sulfur originating from seawater and evaporates, with $\delta^{34}S_{\sum S} \approx +20‰$; (2) sulfur derived from the mantle and deep crust, with $\delta^{34}S_{\sum S} \approx 0‰$; and (3) biogenic sulfur in sedimentary rocks, with $\delta^{34}S_{\sum S}$ values ranging from −20‰ to −10‰ (Machel 1989; Dixon and Davidson 1996). Clearly, our $\delta^{34}S$ values of LAOF stibnite are distinctly different from sulfur originating from seawater, and fall in between the sulfur isotope compositions of the mantle source and of biogenic sulfur in sedimentary rocks. However, while our $\delta^{34}S_{\sum S}$ values of the ore-forming fluid (−4.41‰ to +0.04‰) are mostly negative, they are generally close to the sulfur isotopic composition of the mantle source. Additionally, previous studies have shown that negative $\delta^{34}S$ values in hydrothermal deposits may also result from gas phases (such as H_2S) escaping during fluid boiling (Hagemann et al. 1994; Hodkiewicz et al. 2009). We conclude that sulfur in the LAOF was dominated by a mantle source, with possible involvement of biogenic sulfur.

5.2 The nature of ore-forming fluids and mineral precipitation

Type-I and type-II FIs in stibnite from the LAOF had similar salinities and homogenization temperatures. This suggests that these inclusions were captured by stibnite from the same ore-forming fluid. However, the salinities (1.57 wt%–5.26 wt% NaCl equiv.) and homogenization temperatures (150–180 °C) of the stibnite showed smaller ranges than those of the coexisting quartz (1.91 wt%–5.86 wt% NaCl equiv. and 138.2–251.5 °C, respectively).

It is noteworthy that homogenization temperatures and salinities of FIs in stibnite were consistent with the main peak values of FIs in quartz (170–190 °C and 3.1 wt%–4.5 wt% NaCl equiv., respectively), which suggests that these FIs with relatively high temperature and high salinity were captured by stibnite and quartz at the main-ore stage. This could indicate that the stibnite and coexisting quartz formed under the same geophysical and geochemical conditions. Generally, fluid mixing and boiling are the two most important ore-forming processes for hydrothermal ore deposits (Wilkinson 2001), and the formation of most antimony and gold deposits is related to fluid boiling (e.g., Guillemette and Williams-Jones 1993; Bailly et al. 2000; Zhu and Peng 2015). In our study, evidence of boiling was locally observed in stibnite at the main-ore stage (Fig. 5d, f); a negative correlation between homogenization temperatures and salinities for FIs in stibnite (Fig. 8) further supports boiling as a key mechanism responsible for the precipitation of stibnite at the main-ore stage (Mernagh 2001; Chen 2012; Lawrence et al. 2013). EPMA data show that the As content of pyrite at the late-ore stage sharply decreased. However, the Au content increased compared with stibnite at the main-ore stage, which implies minor Au precipitation during the collapse of the hydrothermal system.

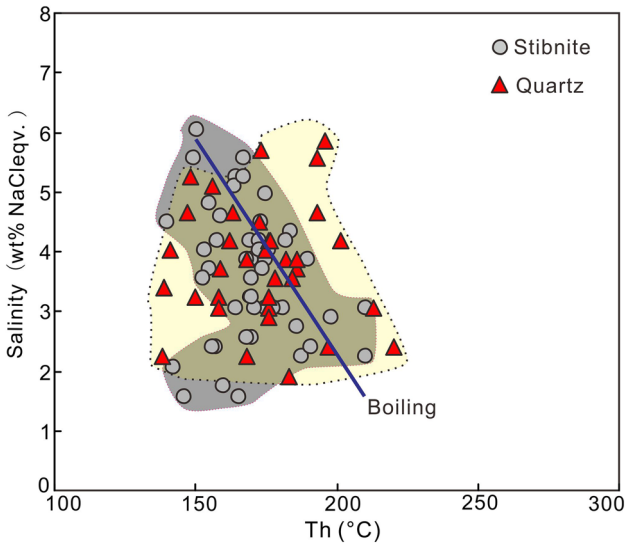

Fig. 8 Diagram of salinity versus homogenization temperatures for the different types of fluid inclusions collected from the Leishan-Rongjiang antimony ore field

Analysis of FIs in stibnite and quartz suggest that the ore-forming fluid was a low-temperature (150–210 °C), low-salinity (1.5 wt%–6.0 wt%. NaCl equiv.) NaCl–H_2O hydrothermal system. The $\delta^{34}S$ data suggest that sulfur was mainly derived from a mantle source. As mentioned previously, the magmatism in this area is not directly related to the Sb mineralization (Wang et al. 1994; Zhang 1994). However, previous studies have shown that the average content of Sb is approximately 15.77 ppm in pre-Sinian Xiajiang Group epimetamorphic rocks (Zhang 1994; Zhang

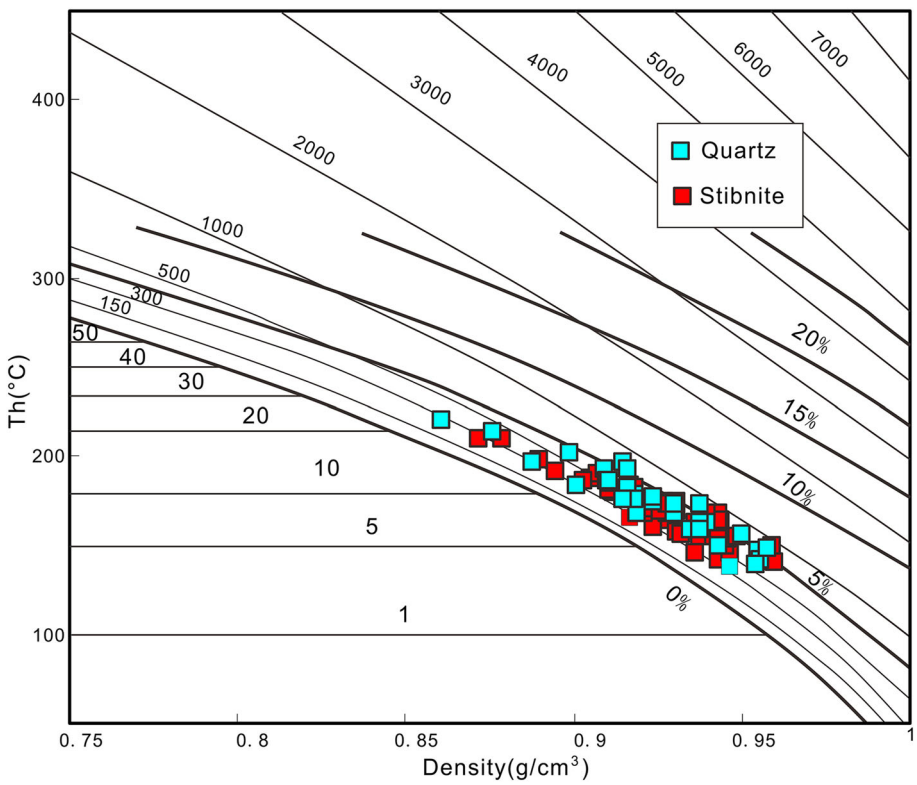

Fig. 9 *D-T-P* diagram of NaCl–H_2O system for fluid inclusions collected from the Leishan-Rongjiang antimony ore field (after Roedder 1984)

Table 4 Characteristics of hydrothermal mineralization of the representative deposits of the South China antimony ore belt

	Youjiang basin	LAOF	Xiangzhong basin
Representative deposits	Qinglong	Bameng and Peize	Woxi
Metallogenic temperature (stibnite) (°C)	220–285	150–210	140–240
Salinity (wt%. NaCleqv)	0.18–19.45	1.5–6.0	<7
Mechanism of fluid precipitation	Fluid mixing	Fluid boiling	Fluid boiling
Wall rock	Pyroclastic rocks of Middle Permian	Neoproterozoic low-grade metamorphic clastic rocks	Neoproterozoic low-grade metamorphic clastic rocks
Alteration	Silicification, fluoritization, pyritization	Silicification, sericitization, pyritization	Silicification, sericitization, pyritization
Ore-controlling structure	Strata-bound	Secondary faults	Interformational faults
Age (Ma)	142–148	About the caledonian	420
The $\delta^{34}S$ value of stibnite (‰)	−3.2 to +3.4	−8.21 to −3.76	−5.85 to −0.90
References	Chen (1991), Peng et al. (2003b), Chen et al. (2014), Su et al. (2015)	This paper	Peng et al. (2002, 2003a), Gu et al. (2004), Zhu and Peng (2015)

et al. 2012). Moreover, boiling is sometimes caused by an abrupt drop in pressure induced by the fault-valve mechanism in hydrothermal systems (Wilkinson 2001) and structural evidence for fluid-pressure fluctuations (Fig. 3) is common in the LAOF. Similarly, the diagram of the homogenization temperature, density, and pressure relationships (*D–T–P*) of the NaCl–H_2O system in stibnite and quartz (Fig. 9) indicates that the pressures of stibnite and quartz FIs were generally between 250 and 800 atmospheres, belonging to the range of low-pressure fluid (Lu et al. 2004). Therefore, it can be concluded that low-temperature, dilute hydrothermal fluids with mixed origins migrated along the regional fault and interacted with the wall rock, extracting the ore-forming materials. Then, through boiling, the ore-forming fluids were injected into the fault fracture zones.

5.3 Implications for the South China Sb metallogenic belt

The South China Sb metallogenic belt is composed of the Youjiang basin antimony ore field, the LAOF, and the Xiangzhong basin from west to east (Fig. 1a). However, the LAOF's location in the uplift between the other two ore fields has significantly restricted understanding of Sb mineralization in South China.

In this paper, which compared the LAOF with typical deposits in the Youjiang and Xiangzhong basins, we found that the Youjiang basin Sb deposit samples (e.g., Qinglong) were characterized by higher temperature and higher salinity and were conspicuously different from the LAOF and Xiangzhong basin deposits (Table 4). However, the LAOF and Xiangzhong Sb deposits exhibited some similar characteristics, including the following: (1) the Sb ore bodies were all hosted in Neoproterozoic low-grade metamorphic clastic rocks; (2) they were formed in a similar metallogenic epoch and geological setting; and (3) the ore-forming fluid was characterized by low homogenization temperature and low salinity, and boiling was the dominant factor affecting mineral precipitation. Thus, we suggest that the Neoproterozoic low-grade metamorphic area in eastern Guizhou Province is a potential target for finding new large antimony deposits.

6 Conclusions

1. Ore-forming fluids in the LAOF were characterized by low temperature (150–210 °C), low salinity (1.5 wt%–6.0 wt% NaCl equiv.), and low density (0.872 and 0.961 g/cm^3).
2. Fluid boiling may have been a key factor responsible for the precipitation of stibnite, and it may have been caused by an abrupt drop in pressure when the ore-forming fluids were injected in the fault fracture zones of the LAOF.
3. The $\delta^{34}S$ values of stibnite ranged from −8.21‰ to −3.76‰ with an average −6.30‰. The $\delta^{34}S_{\sum S}$ values

of the ore-forming fluid varied from −4.41‰ to +0.04‰ (average: −2.49‰), indicating that the sulfur in the LAOF was dominated by a mantle source, but involvement of biogenic sulfur remains a possibility.

Acknowledgments This study was financially supported by the National Natural Science Foundation (Grant No. 41503030) and the Planning Project of Science and Technology Cooperation of Guizhou Province (Grant Nos. 20157663, 20152032). This work was made possible by the assistance of engineers Jiali Cai and Jing Gu during the fluid inclusion and sulfur isotope analyses, respectively. The authors give special thanks to the geologists and miners of the Bameng mining district for their enthusiasm, as well as to the miners of the field investigation.

Compliance with ethical standards

Conflict of interest There is no conflict of interest.

References

Bailly L, Bouchot V, Beny C, Milesi JP (2000) Fluid inclusion study of stibnite using infrared microscopy: an example from the Brouzils antimony deposit (Vendee, Armorican massif, France). Econ Geol 95(1):221–226

Bao ZX (1989) Stratabound antimony deposits in Western Hunan. Miner Depos 8(4):49–60 **(in Chinese with English abstract)**

Bao ZX, Wan RJ, Bao YM (1999) The metallogenetic series of the W-Sb-Au deposits and its stable isotopic research in Western Hunan Province. Beijing Geol 1:11–17 **(in Chinese with English abstract)**

Bodnar RJ (1993) Revised equation and table for determining the freezing-point depression of H_2O–NaCl solutions. Geochim Cosmochim Acta 57(3):683–684

Brown PE, Lamb WM (1989) P–V–T properties of fluids in the system $H_2O \pm CO_2 \pm$ NaCl: new graphical presentations and implications for fluid inclusion studies. Geochim Cosmochim Acta 53(89):1209–1221

Buchholz P, Oberthür T, Lüders V, Wilkinson J (2007) Multistage Au–As–Sb mineralization and crustal-scale fluid evolution in the Kwekwe district, Midlands greenstone belt, Zimbabwe: a combined geochemical, mineralogical, stable isotope, and fluid inclusion study. Econ Geol 102:347–378

Campbell AR, Panter KS (1990) Comparison of fluid inclusions in coexisting (cogenetic?) wolframite, cassiterite, and quartz from St. Michael's Mount and Cligga Head, Cornwall, England. Geochim Cosmochim Acta 54(3):673–681

Chen DY (1991) A research on stable isotopes of major strata-bound Sb–Hg ore deposits in Eastern Yunnan and western Guizhou. Guizhou Geol 3(28):227–240 **(in Chinese with English abstract)**

Chen AQ (2012) Study on mineralization regularity and formation mechanism of scheelite and wolframite in the Woxi Au–Sb–W deposit in Hunan province. Beijing: Chinese University of Geosciences (Beijing). M.Sc. Thesis, pp 1–66

Chen GY, Du HS, Zhang SZ, Huang GS (1991) A preliminsry study of geolgical features and ore-forming geological conditions of the Sb-ore deposit in Bameng of Rongjiang County. Guizhou Guizhou Geol 8(4):302–312 **(in Chinese with English abstract)**

Chen J, Yang RD, Zheng LL, Gao JB, Wei HR (2014) A research on the genesis of the conglomerate of Dachang Layer of Middle Permian in Qinglong. Guizhou Geol Rev 60(6):1309–1322 **(in Chinese with English abstract)**

Chen MH, Mao JW, Li C, Zhang ZQ, Dang Y (2015) Re–Os isochron ages for arsenopyrite from Carlin-like gold deposits in the Yunnan–Guizhou–Guangxi "golden triangle", southwestern China. Ore Geol Rev 64(1):316–327

Dixon G, Davidson GJ (1996) Stable isotope evidence for thermochemical sulfate reduction in the Dugald river (Australia) strata-bound shale-hostedzinc-lead deposit. Chem Geol 129(3–4):227–246

Ge X, Su WC, Zhu LY, Wu LY (2011) A study on the influence of infrared light source intensity on salinity of fluid inclusion in opaque mineral by using infrared microthermometry: in the case of stibnite. Acta Mineral Sin 31(3):366–371 **(in Chinese with English abstract)**

Gu XX, Liu JM, Schulz O, Vavtar F, Zheng MH (2004) Syngenetic origin of the Woxi W–Sb–Au deposit in Hunan: evidence from trace elements and sulfur iostopes. Chin J Geol 39(3):429–439 **(in Chinese with English abstract)**

Guillemette N, Williams-Jones AE (1993) Genesis of the Sb–W–Au deposits at Ixtahuacan, Guatemala: evidence from fluid inclusions and stable isotopes. Mineral Depos 31(3):167–180

Hagemann SG, Gebre-Mariam M, Groves DI (1994) Surface-water influx in shallow-level Archean lode-gold deposits in Western Australia. Geology 22(12):1067–1070

Hodkiewicz PF, Groves DI, Davidson GJ, Weinberg RF, Hagemann SG (2009) Influence of structural setting on sulphur isotopes in Archean orogenic gold deposits, Eastern Goldfields Province, Yilgarn, Western Australia. Mineral Depos 44(2):129–150

Hu RZ, Zhou MF (2012) Multiple Mesozoic mineralization events in South China: an introduction to the thematic issue. Mineral Depos 47(6):579–588

Hu RZ, Su WC, Bi XW, Tu GZ, Hofstra AH (2002) Geology and geochemistry of Carlin-type gold deposits in China. Mineral Depos 37(3):378–392

Hu RZ, Peng JT, Ma DS, Su WC, Shi CH, Bi XW, Tu GZ (2007) Epoch of large-scale low-temperature mineralizations in southwestern Yangtze massif. Miner Depos 26(6):583–596 **(in Chinese with English abstract)**

Huang ZL, Hu RZ, Su WC, Wen HJ, Liu S, Fu YZ (2011) A study on the large-scale low-temperature metallogenic domain in Southwestern China-significance, history and new progress. Acta Mineral Sin 31(3):309–314 **(in Chinese with English abstract)**

Kouzmanov K, Bailly L, Ramboz C, Rouer O, Bény J-M (2002) Morphology, origin and infrared microthermometry of fluid inclusions in pyrite from the Radka epithermal copper deposit, Srednogorie zone, Bulgaria. Mineralium Deposita 37(6–7):599–613

Lawrence DM, Treloar PJ, Rankin AH, Boyce A, Harbidge P (2013) A fluid inclusion and stable isotope study at the Loulo Mining District, Mali, West Africa: implications for multifluid sources in the generation of orogenic gold deposits. Econ Geol 108(2): 229–257

Lu HZ (2014) Fluid inclusion petrography: a discussion. Geol J China Univ 20(2):177–184 **(in Chinese with English abstract)**

Lu HZ, Fan HR, Ni P, Ou G, Shen K, Zhang WH (2004) Fluid inclusion. Science Press, Beijing **(in Chinese)**

Machel HG (1989) Relationships between sulphate reduction and oxidation of organic compounds to carbonate diagenesis, hydrocarbon accumulations, salt domes, and metal sulphide deposits. Carbonate Evaporite 4(2):137–151

Mancano DP, Campbell AR (1995) Microthermometry of enargite-hosted fluid inclusions from the Lepanto, Philippines, high-sulfidation Cu, Au deposit. Geochim Cosmochim Acta 59(19):3909–3916

Mernagh TP (2001) A fluid inclusion study of the Fosterville Mine: a turbidite-hosted gold field in the Western Lachlan Fold Belt, Victoria, Australia. Chem Geol 173(1):91–106

Ni P, Fan HR, Ding JY (2014) Progress in fluid inclusions. Bull Miner Petrol Geochem 33(1):1–5 **(in Chinese with English abstract)**

Ni P, Wang XD, Wang GG, Huang JB, Pan JY, Wang TG (2015) An infrared microthermometric study of fluid inclusions in coexisting quartz and wolframite from Late Mesozoic tungsten deposits in the Gannan metallogenic belt, South China. Ore Geol Rev 65(4):1062–1077

Ohmoto H (1972) Systematics of sulfur and carbon isotopes in hydrothermal ore deposits. Econ Geol 67(5):551–578

Ohmoto H, Goldhaber MB (1997) Sulfur and carbon isotopes. In: Barnes HL (ed) Geochemistry of hydrothermal ore deposits, 3rd edn. Wiley, New York, pp 517–611

Ohmoto H, Rye RO (1979) Isotopes of sulfur and carbon. In: Barnes HL (ed) Geochemistry of hydrothermal ore deposits, 2nd edn. Wiley, New York, pp 509–567

Peng JT, Hu RZ, Lin YX, Zhao JH (2002) Sm–Nd isotope dating of hydrothermal calcites from the Xikuangshan antimony deposit, Central Hunan. Chin Sci Bull 47(13):1134–1137

Peng JT, Hu RZ, Zhao JH, Fu YZ, Lin YX (2003a) Scheelite Sm–Nd dating and quartz Ar–Ar dating for Woxi Au–Sb–W deposit, western Hunan. Chin Sci Bull 48(23):2640–2646

Peng JT, Hu RZ, Jiang GH (2003b) Samarium-Neodymium isotope system of fluorites from the Qinglong antimony deposit, Guizhou Province: constraints on the mineralizing age ore-forming materials'sources. Aata Petrol Sin 19(4):785–791 **(in Chinese with English abstract)**

Roedder E (1984) Fluid inclusions. Miner Soc Am Rev Miner 12:1–644

Saravanan CS, Mishra B (2009) Uniformity in sulfur isotope composition in the orogenic gold deposits from the Dharwar Craton, southern India. Miner Depos 44(5):597–605

Seal RR (2006) Sulfur isotope geochemistry of sulfide minerals. Rev Mineral Geochem 61(1):633–677

Su WC, Xia B, Zhang HT, Zhang XC, Hu RZ (2008) Visible gold in arsenian pyrite at the Shuiyindong Carlin-type gold deposit, Guizhou, China: implications for the environment and processes of ore formation. Ore Geol Rev 33(3–4):667–679

Su WC, Hu RZ, Xia B, Xia Y, Liu YP (2009) Calcite Sm–Nd isochron age of the Shuiyindong Carlin-type gold deposit, Guizhou, China. Chem Geol 258(3–4):269–274

Su WC, Zhang HT, Hu RZ, Ge X, Xia B, Chen YY, Zhu C (2012) Mineralogy and geochemistry of gold-bearing arsenian pyrite from the Shuiyindong Carlin-type gold deposit, Guizhou, China: implications for gold depositional processes. Mineral Depos 47(6):653–662

Su WC, Zhu LY, Ge X, Shen NP, Zhang XC, Hu RZ (2015) Infrared microthermometry of fluid inclusions in stibnite from the Dachang antimony deposit, Guizhou. Aata Petrol Sin 31(4):918–924 **(in Chinese with English abstract)**

Sun XM, Mo RW, Zhai W, Wei HX, Liang YH, Zhang XG, Yi JZ (2014) Infrared fluid inclusion microthemometry on stibnite from Shalagang antimony ore in southern Tibet, China. Aata Petrol Sin 30(1):189–198 **(in Chinese with English abstract)**

Wang SF, Wei JX, Zhang YL (1994) Geology and geochemistry of the Bameng antimony orefield. Geological Publishing House, Beijing **(in Chinese with English abstract)**

Wilkinson JJ (2001) Fluid inclusions in hydrothermal ore deposits. Lithos 55(1–4):229–272

Xiao XG (2014) Geochronology, ore geochemistry and genesis of the Banpo antimony deposit, Guizhou Province, China. Published Ph.D. thesis, Kunming, China, Kunming University of Seience and Technology, 151 p (**in chinese**)

Zhang ZJ (1985) Some remarks on the ore formation laws of stibine (antimony) in Yunan, Guizhou and Guangxi Provinces. Guizhou Geol 3(5):193–204 **(in Chinese with English abstract)**

Zhang YL (1994) Typomorphic characteristics of bameng stibnite and genesis of the ore deposit. Acta Petrol Et Miner 13(4):362–369 **(in Chinese with English abstract)**

Zhang XD, Yang RD, Liu L, Wei HR (2012) Elements geochemistry of the Neoproterozoic Xiajiang group in Jinping Country, Guizhou Province, and its impact on the Gold Deposits. Acta Geol Sin 86(2):258–268 **(in Chinese with English abstract)**

Zheng YF (1991) Sulphur isotopic fractionation between sulphate and sulphide in hydrothermal ore deposits: disequilibrium vs equilibrium processes. Terra Nova 3(5):510–516

Zhu YN, Peng JT (2015) Infrared microthermometric and noble gas isotope study of fluid inclusions in ore minerals at the Woxi orogenic Au–Sb–W deposit, western Hunan. South China. Ore Geol Rev 65(1):L55–L69

Zhu AL, Yi GG, Ma Y, Zheng QL (1999) Metallogenetic regulation of leigongshan antimony deposit of Guizhou. Guizhou Geol 60(3):221–232 **(in Chinese with English abstract)**